NeuroImage 332 (2026) 121899

Contents lists available at ScienceDirect

NeuroImage

journal homepage: www.elsevier.com/locate/ynimg

# Alcohol impacts an fMRI marker of neural inhibition in humans and rodents

Monami Nishio [a,*], Xinyi Wang [b], Eli J. Cornblath [c], Sung-Ho Lee [d], Yen-Yu Ian Shih [d], Nicola Palomero-Gallagher [e,f], Michael J. Arcaro [a], David M. Lydon-Staley [b,g], Allyson P. Mackey [a]

[a] Department of Psychology, School of Arts and Sciences, University of Pennsylvania, Philadelphia, PA, USA
[b] Annenberg School for Communication, University of Pennsylvania, Philadelphia, PA, USA
[c] Department of Neurology, Perelman School of Medicine, University of Pennsylvania, Philadelphia, PA, USA
[d] Center for Animal MRI, University of North Carolina, Chapel Hill, NC, USA
[e] Institute of Medicine, Research Centre, Jülich, D-52425, Germany
[f] C. & O. Vogt Institute of Brain Research, Heinrich-Heine-University Düsseldorf, Düsseldorf, Germany
[g] Leonard Davis Institute of Health Economics, University of Pennsylvania, Philadelphia, PA, USA

ARTICLE INFO

*Keywords:*
Hurst exponent
Pharmacological fMRI
Neural inhibition
Alcohol
$GABA_A$ receptor
Cross-species

ABSTRACT

Inhibitory neuronal activity is a key regulator of brain function and is implicated in numerous developmental and psychiatric disorders. However, measuring inhibition *in vivo* remains a challenge. The Hurst exponent of the fMRI signal has been shown to correlate spatially with cellular measures of neural inhibition, but there have been few causal tests of the relationship between the Hurst exponent and neural inhibition. Here, we used alcohol, a drug with known impacts on inhibition, as a way to evaluate the validity of the Hurst exponent as a marker of neural inhibition across rats and humans. In rats, acute alcohol administration significantly reduced the cortical Hurst exponent, with the spatial distribution of effects closely aligned with $GABA_A$ receptor expression. In humans, alcohol exposure similarly decreased the cortical Hurst exponent, particularly in regions with high $GABA_A$ receptor expression, demonstrating cross-species consistency. These results provide convergent*in vivo* evidence that the Hurst exponent is sensitive to pharmacologically induced changes in inhibitory neuronal activity.

## 1. Introduction

Inhibitory neuronal activity is increasingly recognized as a critical regulator of brain plasticity (Hensch, 2005), and its disruption has been linked to a wide range of developmental and psychiatric disorders, including autism (Trakoshis et al., 2020), schizophrenia (Liu et al., 2021), and depression (Gerner and Hare, 1981). Additionally, early life adversity, including maltreatment (Hanson and Nacewicz, 2021) and prenatal exposure to substances such as alcohol (Shenoda, 2017) and cocaine (McCarthy et al., 2011) can impact inhibitory development. However, direct measurement of neural inhibition in the living human brain remains a major challenge. Magnetic resonance spectroscopy can estimate GABA levels *in vivo* (Tognarelli et al., 2015), but it can only measure one large voxel at a time, making it unsuitable for whole-brain analysis. An emerging alternative is the Hurst exponent (Chini et al., 2022; Gao et al., 2017; Trakoshis et al., 2020), which quantifies long-range temporal correlations and scale-invariant dynamics in various time series including fMRI (Linkenkaer-Hansen et al., 2001). Computational models have demonstrated that enhancing inhibitory neuronal activities leads to an increase in the Hurst exponent of simulated local field potential and BOLD signals (Chini et al., 2022; Gao et al., 2017; Lombardi et al., 2017; Trakoshis et al., 2020). One possible explanation is that inhibitory activity stabilizes local network dynamics by suppressing spontaneous excitatory fluctuations and neural noise. This stabilization can produce more temporally structured neural activity with stronger long-range temporal dependencies, resulting in higher Hurst exponent values (Lombardi et al., 2017; Trakoshis et al., 2020). Conversely, reduced inhibitory control may lead to more irregular and less temporally dependent neural signals, producing lower H values. Local field potential data in mice have been used to show that regions with higher GABA synapse density have higher Hurst exponents, indicating a spatial relationship between the inhibitory synaptic density and the Hurst exponent (Gao et al., 2017). We have recently shown a strong spatial correlation between PV inhibitory neurons and the Hurst

* Corresponding author.
*E-mail address:* monami@sas.upenn.edu (M. Nishio).

https://doi.org/10.1016/j.neuroimage.2026.121899
Received 22 September 2025; Received in revised form 19 March 2026; Accepted 30 March 2026
Available online 31 March 2026

exponent across the cortex in both humans and rodents, suggesting that the Hurst exponent reflects inhibitory neurons across species (Nishio et al., 2025). Collectively, these findings suggest that the Hurst exponent is a promising whole-brain marker of inhibitory neural activity. However, evidence to date is largely correlational.

A critical next step is to test the causal validity of the Hurst exponent as a marker of neural inhibition. Here, we apply the framework of pharmacological fMRI (Kotoula et al., 2023; Larsen et al., 2022), using alcohol as the pharmacological challenge. Alcohol offers a unique opportunity to study neural inhibition in humans because of its widespread use and well-characterized effects on the brain. Acute alcohol consumption induces cognitive disinhibition, significantly increasing various health and social risks (National Highway Traffic Safety Administration, 2022; Sontate et al., 2021). This alcohol-induced disinhibition is often associated with weakened top-down control due to suppression of neuronal activity (Fernando Valenzuela, 1997). Rodent studies indicate that alcohol suppresses both excitatory (Badanich et al., 2013; Nimitvilai et al., 2017) and inhibitory neuronal activity (Woodward and Pava, 2009), but through distinct mechanisms: suppression of excitatory neurons is mediated primarily by antagonistic effects on NMDA receptors (Badanich et al., 2013; Li et al., 2002), whereas suppression of inhibitory neurons is mediated primarily by agonistic effects on $GABA_A$ receptors (Diaz and Valenzuela, 2016; Jia et al., 2008; Liang et al., 2006). In humans, alcohol produces widespread changes in cerebral blood flow (Marxen et al., 2014; Mathew and Wilson, 1986; Rickenbacher et al., 2011; Strang et al., 2015) and functional connectivity (Broadwater et al., 2018; Han et al., 2021; Lee et al., 2023; Ochi et al., 2022), particularly in visual (Esposito et al., 2010; Khalili--Mahani et al., 2012; Ochi et al., 2022), sensorimotor (Ochi et al., 2022), and frontoparietal networks (Han et al., 2021). Given alcohol's suppressive effects on inhibitory neurons observed in rodents, together with its widespread effects on the human brain reported in neuroimaging studies, we expect alcohol to reduce the Hurst exponent across cortical regions.

Here, we use alcohol to validate the Hurst exponent as an fMRI marker of neural inhibition. We first examine alcohol's impact on the Hurst exponent in genetically and environmentally consistent, alcohol-naive, and age-controlled rodents to minimize individual variability. We also explore the correlation between alcohol's effect on the Hurst exponent and $GABA_A$ receptor expression across the cortex, shedding light on the receptors likely contributing to alcohol's impact on neural inhibition. Next, we test the replicability of these findings in humans using an extensive repeated-measures (10 session) dataset. Together, these cross-species analyses provide *in vivo* evidence that the Hurst exponent is sensitive to pharmacologically induced changes in neural inhibition, advancing the validation of this novel fMRI marker.

## 2. Methods

### 2.1. Rat data and analyses

#### 2.1.1. Imaging subjects

The data analyzed in this study were previously published by Lee et al. (Lee et al., 2023). Briefly, a total of 38 Wistar rats, bred and reared in-house, were included in the experiment. The pups remained with their mother until weaning at postnatal day 21 (P21), and were subsequently scanned at either postnatal day 45 (P45; $N = 19$, 11 females) or postnatal day 80 (P80; $N = 19$, 10 females). All animals were maintained in a temperature- and humidity-controlled vivarium under a 12:12 h light-dark cycle, with *ad libitum* access to food and water.

#### 2.1.2. Experimental design

Each animal underwent a single scanning session at age P45 or P80. During each session, a total of 75 min of resting-state fMRI were collected, divided into five 15-minute blocks. After the first 15 min of baseline scanning, animals received an intraperitoneal injection of saline, followed by two 1 g/kg and one 2 g/kg injections of 20 % v/v ethanol, with one injection administered per 15-minute block (Shnitko et al., 2016, 2014).

#### 2.1.3. MRI data acquisition

All MR images were acquired at the UNC Center for Animal MRI on a Bruker BioSpec 9.4-T, 30 cm bore system using an 86 mm volume coil (RF transmitter) and 4-channel receiver. BOLD resting-state fMRI data were collected with a 2D multi-slice, single-shot, gradient-echo EPI sequence (TR = 2000 ms, TE = 14 ms, flip angle = 70°, FOV = 28.8 × 28.8 mm, matrix = 72 × 72, 32 slices, 0.4 mm isotropic voxels). Rats were initially anesthetized with 4 % isoflurane, which was then reduced to 2 % for secure placement in an MR-compatible rat cradle. Once stabilized, a continuous infusion of dexmedetomidine (0.05 mg/kg/hr) and pancuronium bromide (0.5 mg/kg/hr) was administered, while isoflurane was further reduced to 0.5 %. This infusion protocol was initiated 30 min prior to the start of fMRI scans (Lu et al., 2012).

#### 2.1.4. MRI data preprocessing

To focus on steady-state data, we excluded the first 5 min of each block containing the injection periods, analyzing only the final 10 min of each block. All fMRI data were first corrected for slice timing and motion using AFNI (Cox, 1996). Time-averaged images were used to generate brain masks via an in-house 2D-UNET algorithm (Hsu et al., 2020) and manually refined with ITK-SNAP (Yushkevich et al., 2006). These masks were applied to the corresponding fMRI data to remove non-brain signals, followed by spatial normalization to an in-house EPI template using ANTs SyN registration (Avants et al., 2008). Nuisance signals, including baseline trends and six motion parameters, were regressed out, and the data were band-pass filtered (0.01–0.1 Hz) and smoothed with a 0.5 mm FWHM Gaussian kernel. Each session was divided into five 15-minute blocks corresponding to different exposure periods. Data were parcellated using a functional rat brain atlas (Lee et al., 2021), and time courses were averaged within parcels to calculate the Hurst exponent. Averaging signals within parcels reduces voxel-level noise and improves the robustness of group-level estimates. Previous studies have shown that region-averaged Hurst exponent values capture spatial patterns of scale-free brain dynamics that are highly consistent with voxel-level analyses, while providing greater stability for comparisons across subjects and conditions (Churchill et al., 2016; He, 2011; Wink et al., 2008). Correspondence between parcels and anatomical regions is provided in Table S1 (Lee et al., 2021). Functional parcels are named according to the anatomical regions with which they show the greatest overlap. Three animals showed outlier levels of motion (mean Fig displacement exceeding 3 standard deviations above the mean) and were therefore excluded.

#### 2.1.5. Hurst exponent

The Hurst exponent can be estimated using several methods. The Power Spectral Density method leverages the relationship between the spectral density of the form $1/f^{\beta}$ and the Hurst exponent $\alpha$, where $\beta = 2\alpha - 1$ (Ivanov et al., 2001). Alternatively, Detrended Fluctuation Analysis estimates the Hurst exponent by quantifying how fluctuations in a detrended, integrated time series scale with the size of the observation window, providing robustness against nonstationarities commonly present in neural data (Chen et al., 2005; Hu et al., 2001; Peng et al., 1994; Schmitt et al., 2009; Schmitt and Ivanov 2007). Finally, fractional integration models treat the time series as fractionally integrated processes, where the Hurst exponent H is defined as $H = d + 0.5$, with $d$ representing the fractional integration order (Linke et al., 2024; Trakoshis et al., 2020; You et al., 2012). In these models, the autocorrelation function (ACF) decays according to a power law, approximately as ACF $(k) \sim k^{2d-1}$, where $k$ is the lag. This means that for $d > 0$, the correlations between distant observations decline slowly, reflecting long-range dependence or persistence in the signal. For this study, we employed the fractional integration model because it is particularly

well-suited for short, noisy fMRI time series. Fractional integration model provides robust, unbiased, and consistent estimates of the Hurst exponent, even in the presence of nonstationarities and measurement noise, and allow for accurate characterization of long-range dependencies in the signal (Flandrin, 1992; Rehman and Mandic, 2010). The Hurst exponent was computed using the *nonfractal* MATLAB toolbox (https://github.com/wonsang/nonfractal) (Trakoshis et al., 2020; You et al., 2012). The specific function utilized is bfn_mfin_ml.m function with the 'filter' argument set to 'haar' and the 'ub' and 'lb' arguments set to [1.5,10] and [−0.5,0], respectively. This toolbox uses a discrete wavelet transform and a model of the time series as fractionally integrated processes and is estimated using maximum likelihood estimation.

#### 2.1.6. Alcohol effect modeling

To model the effect of alcohol, we employed a linear mixed-effects approach. For each parcel, we constructed a model using the formula `Regional Hurst exponent ~ Run + Age + Sex + mean framewise displacement + (1 | Subject)`, where the run (saline, dose1, dose2, dose3), age, sex, and mean framewise displacement were treated as fixed effects. We selected the saline condition as the control instead of the baseline condition to eliminate the influence of the injection procedure on the Hurst exponent. Random intercepts were modeled for each subject to account for repeated measures. The fixed effect of alcohol was extracted and its significance was calculated through an ANOVA test. The *p* values were corrected for multiple comparisons using the false discovery rate method, applied separately to cortical and subcortical parcels.

#### 2.1.7. Correlation with receptor expression

For the correlation analysis between alcohol effects and receptor expression, we used receptor autoradiographs previously published by Palomero-Gallagher et al. (Palomero-Gallagher et al., 2010, 2008). Eight adult male LEW/Ztm rats were included in the study, with serial 20 μm coronal sections obtained at Bregma levels 4.20, 1.56, −2.76, and −4.80 (Paxinos and Watson, 2014). Sections were alternately stained for cell bodies using a modified silver Nissl-staining method or processed for quantitative *in vitro* autoradiography for receptor visualization. Receptor labeling involved pre-incubation in a Tris-citrate buffer to remove endogenous substances, incubation with [$^3$H]-flumazenil to identify total binding sites, and a rinsing step to stop the binding process. Sections were exposed to beta-radiation-sensitive films alongside calibrated microscales to enable densitometric analysis of the ensuing receptor autoradiographs. The autoradiographs were digitized, their grey values converted into receptor densities (fmol/mg protein) by means of the microscales. Regions of interest were manually annotated on the color-coded images according to the cortical parcellation by Haghir et al. (Haghir et al., 2023). Receptor densities were then extracted from these annotated images using the AnaRec software (Impieri et al., 2019).

Based on the correspondence between functional parcels (Lee et al., 2021) and anatomical regions (Table S1), we estimated $GABA_A$ receptor expression for each parcel by aggregating the values from the regions within that parcel and calculating their average. This yielded receptor density data for 30 of the 50 parcels. We then computed Pearson correlations between the fixed effect of alcohol on the Hurst exponent, extracted from the linear mixed-effects model, and $GABA_A$ receptor expression across these 30 parcels.

### 2.2. Human data and analyses

#### 2.2.1. Imaging participants

All participants provided written informed consent, and all procedures were approved by the University of Pennsylvania Institutional Review Board. Adults were included in the study if they were over the age of 21, have consumed at least 1 beverage containing alcohol during the 6 months before their first scan and have no physical conditions that could be influenced by drinking alcohol. Exclusion criteria included women who were pregnant, planning a pregnancy, or lactating. Individuals with a history of cancer, heart disease, stroke, or myocardial infarction within the past six months were also excluded. Participants with contraindications against fMRI, a history of problematic alcohol use (defined as an Alcohol Use Disorders Identification Test score of 8 or higher) (Saunders et al., 1993) or liver disease were not eligible. Additionally, individuals taking medications for which alcohol use is contraindicated, as outlined by the National Institute on Alcohol Abuse and Alcoholism, were excluded from the study (National Institute on Alcohol Abuse and Alcoholism, 2022). Following these criteria, 11 participants were included in the study ($M = 28.1$ years, $SD = 3.26$ years; 4 women, 7 men; 3 identified as Asian, 5 identified as White, 1 identified as White and Hispanic or Latinx).

#### 2.2.2. Experimental design

Participants attended one baseline survey visit and 10 laboratory visits where each session included surveys and an MRI session. For 5 of the visits, participants were asked not to consume alcohol 12 h before the visit and not to eat food for 3 h prior to session. They were then provided with alcoholic beverages designed to increase their blood alcohol content (BAC) to 0.08 % before they underwent MRI. The beverages were consisted of vodka and orange juice mixed in a 3:1 juice: alcohol ratio. The amount consumed was equivalent to approximately 3 standard drinks of alcohol, though it was slightly more or less depending on the participant's age, gender, height, and weight as calculated through a BAC calculator (https://dionysus.psych.wisc.edu/open/bac_calc.html). Participants consumed the beverage within 30 min and were immediately scanned, with BAC measured by breathalyzer before and after the MRI. For the other 5 visits, participants were not provided with alcoholic beverages prior to the MRI scan. Among the 11 participants, one completed an additional non-alcohol session, resulting in a total of 5 alcohol and 6 non-alcohol sessions. One participant completed only five scans (2 alcohol and 3 non-alcohol sessions), and another completed only four scans (2 alcohol and 2 non-alcohol sessions). The two participants who did not complete all 10 sessions left the study because their eligibility for participating in the study changed ($N = 1$) and because they could no longer make time for the study ($N = 1$). The ordering of alcohol and non-alcohol sessions was randomized for each participant.

#### 2.2.3. MRI data acquisition

Imaging data were acquired at University of Pennsylvania on a 3T Siemens Magnetom Prisma scanner equipped with a 32-channel head coil. High-resolution T1-weighted structural images were obtained using a multi-echo magnetization-prepared rapid gradient-echo (MEMPRAGE) sequence (repetition time (TR) = 2530 ms, echo time (TE) = 1.69/3.55/5.41/7.27 ms, TI = 1330 ms, FA (degree) = 7°, field of view (FoV) = 256 mm$^2$, voxel-size =1 mm$^3$, slice thickness = 1 mm, echo spacing = 11.1 ms, bandwidth = 650 Hz/pixel, and acquisition time = 5.26 min). During the structural scan, participants watched a 7-minute video featuring abstract shapes and moves in slow continuous transitions (Vanderwal et al., 2015) in order to help reduce movement, boredom and nervousness. For resting-state fMRI, 60 transversal slices were acquired by using an echoplanar imaging sequence (TR = 800 ms, TE = 30 ms, FA (degree) = 52°, field of view (FoV) = 216 mm$^2$, voxel-size = 2.4 mm$^3$, slice thickness = 2.4 mm, echo spacing = 0.51 mm, multiband acceleration factor = 6, bandwidth =2778 Hz/pixel, and acquisition time = 7.04 min). Each session included four resting-state scans with 2 fixation resting-state scans and 2 film clip resting-state scans. For this study, we only used the fixation resting-state scans. During these scans, a white fixation cross was presented on a black screen.

#### 2.2.4. MRI data preprocessing

The T1-weighted (T1w) image underwent intensity nonuniformity correction using N4BiasFieldCorrection (Tustison et al., 2010) from the Advanced Normalization ToolS (ANTS) version 2.2.0, and used as T1w

reference throughout the workflow. Following this, skull stripping was performed using the antsBrainExtraction.sh script (ANTS version 2.2.0), with the OASIS template as the target. The brain mask was refined with a custom variation of the method to reconcile ANTS-derived and FreeSurfer (Dale et al., 1999) -derived segmentations of the cortical gray matter of Mindboggle (Klein et al., 2017). Spatial normalization to the ICBM 152 Nonlinear atlases version 2009c (Fonov et al., 2011) was performed through nonlinear registration with antsRegistration (Avants et al., 2010), using brain-extracted versions of both T1w volume and template. Brain tissue segmentation of cerebrospinal fluid, white matter, and gray matter was performed on the brain-extracted T1w using Functional MRI of the Brain Software Library (FSL) version 5.0.9 (Zhang et al., 2001).

For each resting-state fMRI run, a reference volume and its skull-stripped version were generated using a custom methodology of fMRIPrep version 20.2.0 (Esteban et al., 2019), which is based on Nipype version 1.1.7 (Gorgolewski et al., 2016). Brain surfaces were reconstructed using the recon-all command (Dale et al., 1999) before other processing, and reconstructed surfaces were used as input to fMRIprep. The BOLD reference was then coregistered to the T1w reference using bbregister (FreeSurfer), employing boundary-based registration (Greve and Fischl, 2009). Coregistration was configured with nine degrees of freedom to account for distortions remaining in the BOLD reference. Head-motion parameters with respect to the BOLD reference (transformation matrices and six corresponding rotation and translation parameters) were estimated before any spatiotemporal filtering using the mcflirt tool (Jenkinson et al., 2002), and slice-time correction was performed using 3dTshift from AFNI 20,160,207 (Cox and Hyde, 1997). The BOLD time series were resampled onto the MNIPediatricAsym standard space by applying a single, composite transform, generating a preprocessed BOLD run in MNI152NLin6Asym space.

Several confounding time series were calculated based on the preprocessed BOLD, including framewise displacement, root-mean-square intensity difference from one volume to the next, and three region-wise global signals (cerebrospinal fluid, white matter, and the whole brain). Framewise displacement and root-mean-square intensity difference were calculated for each functional run, both using their implementations in Nipype (Power et al., 2014). The head-motion estimates calculated in the correction step were also placed within the corresponding confounds file. All resamplings were performed with a single interpolation step (*i.e.*, head-motion transform matrices and coregistrations to anatomic and template spaces).

Further preprocessing of BOLD was implemented in XCP-D 0.5.0 (Ciric et al., 2018), a multimodal tool kit that includes tools from FSL (Jenkinson et al., 2002) and AFNI (Cox, 1996). Preprocessed functional time series on the cortical surface underwent nuisance regression, using a 36-parameter model that included three global signals (whole brain, cerebrospinal fluid, and white matter) and six motion parameters, as well as their derivatives, quadratic terms, and derivatives of quadratic terms. Linear regression, implemented in Scikit-Learn (0.24.2), was employed to regress the confounds. Motion censoring was applied, with outlier volumes exceeding framewise displacement = 0.3 mm flagged and removed from confound regression. The interpolated BOLD data replaces high-motion outlier volumes with cubic spline–interpolated values generated in *nilearn*. Any outlier volumes at the beginning or end of the run were replaced with the closest non-outlier volume's data. If there were <100 s of data remaining after removing high-motion outlier volumes, those runs are excluded. Data were parcellated using a Schaefer 100 parcellation (Schaefer et al., 2018), and time courses were averaged within parcels to calculate the Hurst exponent.

#### 2.2.5. Hurst exponent

We used the same metrics as those applied to rats to calculate the Hurst exponent for humans.

#### 2.2.6. Alcohol effect modeling

To model the effect of alcohol on the Hurst exponent, we employed a linear mixed-effects approach to account for the nested nature of the data (*i.e.*, several runs nested in 11 participants) using the `lmer` function from the `lme4` package in R. For each brain region in the dataset, we constructed a model with the form `Regional Hurst exponent ~ Alcohol + psm_mean_fd + wps_mean_fd + Gender + (1 + Alcohol | Subject)`, where alcohol condition (alcohol / non-alcohol session), psm_mean_fd (person-average mean framewise displacement), wps_mean_fd (run-specific variation from the person-average mean framewise displacement), and gender were treated as fixed effects, while a random slope and intercept for alcohol were included for each subject to account for individual variability in the response to alcohol. The optimization was performed using the "optimx" method with the "nlminb" algorithm. For each region, we extracted the fixed effect of alcohol and calculated its significance through an ANOVA test. The p-values were then corrected for multiple comparisons using the false discovery rate method.

#### 2.2.7. Alignment with the sensorimotor-association axis

We used the Sensorimotor-Association axis derived by Sydnor and colleagues (Sydnor et al., 2021). This map encompasses various cortical hierarchies, including functional connectivity gradients, evolutionary cortical expansion patterns, anatomical ratios, allometric scaling, brain metabolism measures, perfusion indices, gene expression patterns, primary modes of brain function, cytoarchitectural similarity gradients, and cortical thickness.

#### 2.2.8. Correlation with receptor expression

For the correlation analysis between alcohol effects and receptor expression, we used a Positron emission tomography (PET) dataset published by Hansen et al. (Hansen et al., 2022). Volumetric PET images were collected for 19 different neurotransmitter receptors and transporters across multiple studies. These images provide an estimate proportional to receptor densities, so we refer to the measured values (such as binding potential and tracer distribution volume) simply as receptor density. All PET images were registered to the MNI-ICBM 152 non-linear 2009 (version c, asymmetric) template and parcellated into 100 regions according to the Schaefer atlas. To calculate the correlation between alcohol's effect and $GABA_A$ receptor expression across the cortex, we computed the Pearson correlation between the fixed effect of alcohol on the Hurst exponent, derived from the linear mixed-effects model, and PET-based $GABA_A$ receptor expression across 100 cortical parcels.

#### 2.2.9. Spin-based spatial permutation testing

To address distance-dependent spatial autocorrelation in cortical data, we evaluated the significance of Pearson's correlations between two whole-brain cortical feature maps (the Hurst exponent) using non-parametric spin tests. These tests, also known as spatially constrained rotation tests, compare the observed correlation to a null distribution obtained by spatially iterating (spinning) one of the feature maps. Specifically, the null distribution is generated by rotating spherical projections of one map while preserving its spatial covariance structure. The *P* value ($P_{spin}$) is determined by comparing the empirical correlation to the distribution obtained from 10,000 spatial rotations. Spin tests were conducted using the spin permutation test algorithm available in the ENIGMA toolbox for Python (https://enigma-toolbox.readthedocs.io/en/latest/pages/08.spintest/index.html).

## 3. Results

### 3.1. Alcohol exposure reduces the hurst exponent in rats

First, we examined the effect of alcohol on the Hurst exponent in anesthetized rats. Using fractional integration models (Linke et al., 2024; Trakoshis et al., 2020; You et al., 2012), we computed the

autocorrelation function of the time series for each cortical parcel, estimated the fractional integration order ($d$), and the Hurst exponent calculated as $H = d + 0.5$ (Fig. 1A). Rats underwent sequential saline and ethanol injections during the scanning session (Fig. 1 B). After the 2 g/kg and 4 g/kg ethanol injections, the Hurst exponent significantly decreased compared to the first dose, saline, or baseline across the whole brain (Fig. 1 C, ANOVA $F = 17.506$, $P < 0.001$). Region-specific effects were examined across cortical parcels (Fig. 1 D). The effect of alcohol remained significant after multiple comparison correction with $P < 0.05$ in many brain regions across sensory, limbic, and association areas (Fig. 1 E). The effect was particularly strong in sensory and limbic regions, including auditory, visual, temporal and entorhinal regions (Fig. 1 E). Although there was a significant effect of alcohol dose (saline, and 1, 2, 4 g/kg) on mean framewise displacement (Fig. S1A, ANOVA $F =$

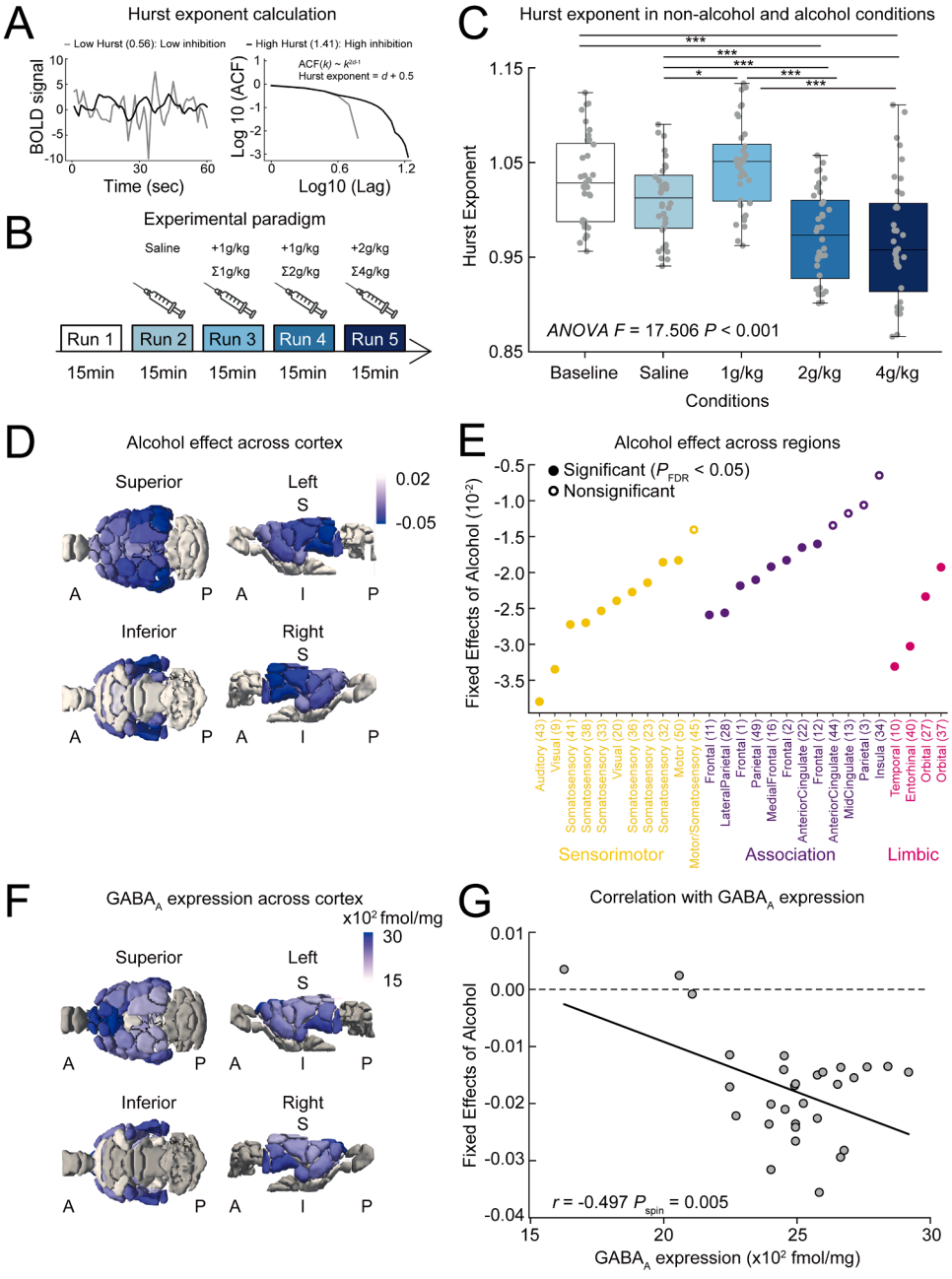


**Fig. 1.** Alcohol's effect on the Hurst exponent in rats. (A) Examples of fMRI time series with high and low Hurst exponents and autocorrelation function (ACF). ACF decays according to a power law, approximately as ACF ($k$) $\sim k^{2d-1}$, where $k$ is the lag. H is defined as $H = d + 0.5$, with $d$ representing the fractional integration order. (B) Schematic illustration of the experimental paradigm for rats. (C) The whole-brain averaged Hurst exponent in rats under different conditions (ANOVA $F =$ 17.506, $P < 0.001$). To control for motion, we regressed out the framewise displacement mean from the original Hurst values and added the residuals to the average Hurst exponent. Post-hoc Tukey HSD test $^{***}P < 0.001$, $^{**}P < 0.01$, $^{*}P < 0.05$. (D) Alcohol's effect across the cortex in rats. (E) Alcohol's effect in sensorimotor (yellow), association (purple) and limbic (pink) regions. Colored filled dots indicate parcels with a significant alcohol effect that survived multiple comparison correction, while unfilled dots represent parcels with non-significant effects. Numbers in parentheses refer to parcel IDs listed in Table S1. The correspondence between functional parcels and anatomical regions is provided in Table S1. (F) Cortical $GABA_A$ receptor expression as visualized *in vitro* by means of the radioligand [$^3$H]-flumazenil. (G) Correlation between alcohol's effect and $GABA_A$ receptor expression across the cortex ($r = -0.497$, $P_{spin} = 0.005$).

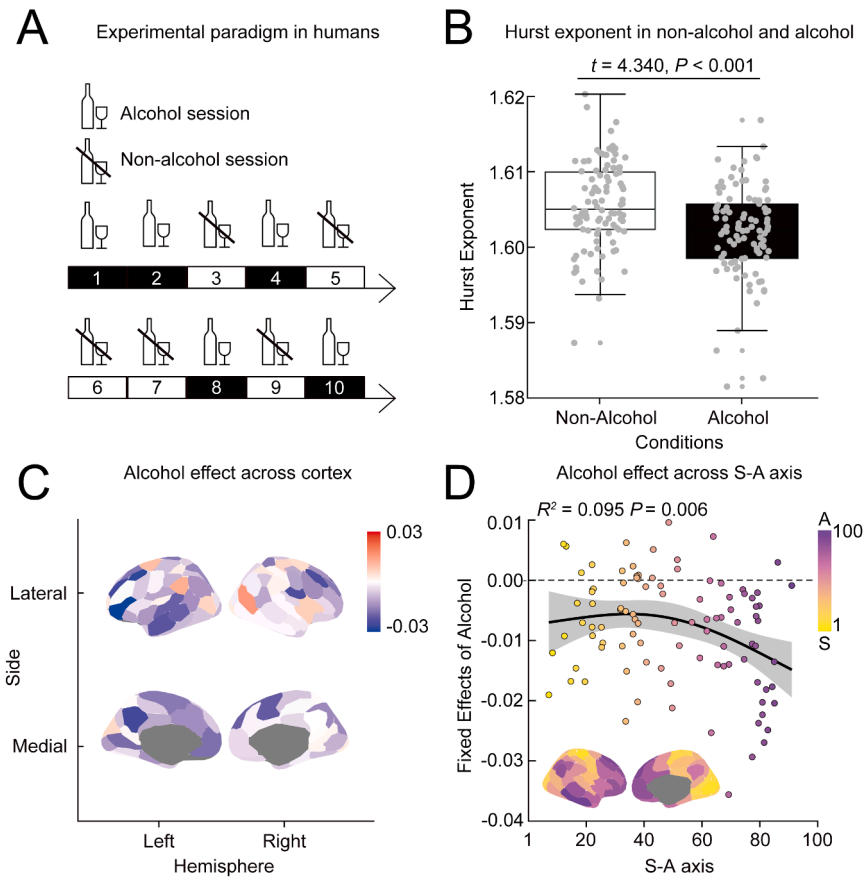


**Fig. 2.** Alcohol's effect on the Hurst exponent in humans. (A) Schematic illustration of the experimental paradigms for humans. Healthy adults (ages 24–33) participated in 10 laboratory sessions—five with alcohol and five without. The order of alcohol and non-alcohol sessions was randomized. (B) The whole-brain averaged Hurst exponent in humans under non-alcohol (white) and alcohol (black) conditions ($t$ = 4.340, $P$ < 0.001). To control for motion, we regressed out the mean framewise displacement from the original Hurst values and added the residuals to the average Hurst exponent. (C) Alcohol's effect across the cortex. (D) Mapping of alcohol's effect along the sensory (yellow) -association (purple) axis ($R^2$ = 0.095, $P$ = 0.006).

4.576, $P$ = 0.002), the Hurst exponent did not correlate with motion at any dose (Fig. S1B, $P$s > 0.069). We controlled for mean framewise displacement for subsequent analysis.

Since previous research suggests that alcohol's effects on inhibitory neurons are primarily mediated through $GABA_A$ receptors (Diaz and Valenzuela, 2016; Jia et al., 2008; Liang et al., 2006), we explored the correlation between alcohol's effect on the Hurst exponent and $GABA_A$ receptor expression across the cortex (Fig. 1 F). There was a significant negative correlation between alcohol's effect on the Hurst exponent and $GABA_A$ receptor expression (Fig. 1 G, $r$ = -0.497, $P_{spin}$ = 0.005), indicating that regions with higher $GABA_A$ receptor expression showed a greater reduction in the Hurst exponent. This result aligns with the previous findings that alcohol's effect on inhibitory neurons is mainly mediated by $GABA_A$ receptors (Diaz and Valenzuela, 2016; Jia et al., 2008; Liang et al., 2006).

Subcortical regions also exhibited a significantly lower Hurst exponent after 2 g/kg or 4 g/kg ethanol injections (Fig. S2A, ANOVA $F$ = 9.109, $P$ < 0.001). After multiple comparison correction, several parcels within the cerebellum, striatum, and amygdala showed significant effect of alcohol (Fig. S2B).

### 3.2. Alcohol exposure reduces the hurst exponent in humans

We next investigated whether alcohol impacts the Hurst exponent in humans using repeated alcohol and non-alcohol sessions (Fig. 2 A). Since alcohol increased participant movement (Fig. S3A, B, $t$ = -3.677, $P$ < 0.001), and the Hurst exponent significantly correlated with motion (Fig. S3C, Non-alcohol; $r$ = -0.811, $P$ < 0.001, Alcohol; $r$ = -0.814, $P$ < 0.001), we excluded sessions with a mean framewise displacement greater than 0.3 mm (Fig. S3C) and controlled for mean framewise displacement for subsequent analysis. Consistent with rodent findings, the average cortical Hurst exponent was significantly lower during alcohol sessions compared to non-alcohol sessions (Fig. 2 B, $t$ = 4.340, $P$ < 0.001). This reduction remained significant using stricter motion exclusion criteria (mean framewise displacement < 0.2) (Fig. S3D, E, $t$ = 3.140, $P$ = 0.002). Although no parcels survived multiple comparison correction over 100 parcels, the effect was consistently negative across the cortex (Fig. 2 C). The most pronounced decreases were observed in association regions (Fig. 2 D, Generalized Additive Model $R^2$ = 0.095, $P$ = 0.006). This pattern remained even when non-alcohol sessions were subsampled to balance session counts between alcohol and non-alcohol sessions (Fig. S3F, $R^2$=0.063, $P$ = 0.029).

We next asked whether the effects of alcohol were correlated with $GABA_A$ receptor distribution. $GABA_A$ receptors show particularly strong expression at both ends of the Sensorimotor-Association axis (Fig. 3 A, B, $R^2$ = 0.144, $P$ < 0.001). Consistent with rodent findings, $GABA_A$ receptor expression significantly negatively correlated with alcohol's effect on the Hurst exponent. The correlation between alcohol's effect and $GABA_A$ receptor expression remained significant even after controlling for the Sensorimotor-Association axis with partial correlation test (Fig. 3 C $r$ =

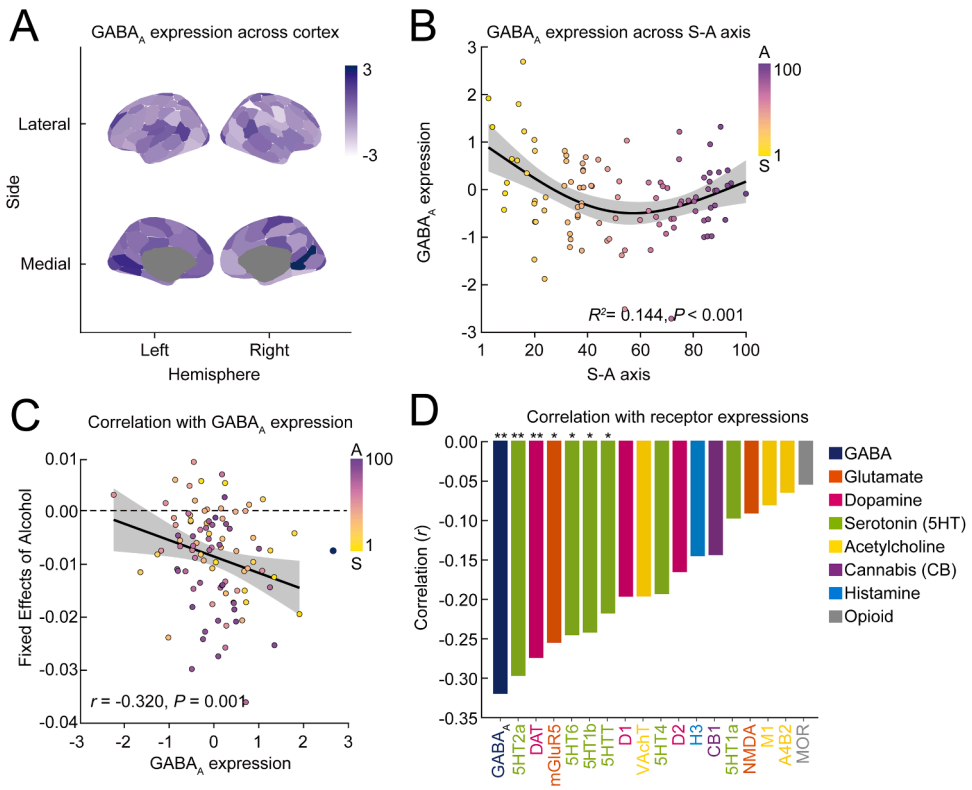


**Fig. 3.** Alcohol's effect on the Hurst exponent in humans. (A) $GABA_A$ receptor expression across the cortex (z-scored). (B) Mapping of $GABA_A$ receptor expression along the Sensorimotor (yellow) -Association (purple) axis ($R^2 = 0.144$, $P < 0.001$). (C) Correlation between alcohol effects and $GABA_A$ receptor expression across the cortex. Sensorimotor-Association rank is controlled using partial correlation test ($r$ = -0.320, $P$ = 0.001). (D) Correlation coefficients between alcohol effects and receptors, controlling for Sensorimotor-Association rank. *$P$ < 0.05, **$P$ < 0.01. $GABA_A$; gamma-aminobutyric acid type A receptor, mGluR5; metabotropic glutamate receptor 5, NMDA; n-methyl-d-aspartate receptor, DAT; dopamine transporter, D1,2; dopamine receptor 1,2, 5HT1a,1b,2a,4,6; 5-hydroxytryptamine (serotonin) receptor, 5HTT; serotonin transporter, VAchT; vesicular acetylcholine transporter, CB1; cannabinoid receptor type 1, H3; histamine receptor H3, MOR; mu-opioid receptor.

-0.320, $P$ = 0.001), indicating that the Sensorimotor-Association axis does not fully explain this relationship. We also examined the correlation between alcohol effects and the expression of other receptors, uptake sites and transporters (Hansen et al., 2022) while controlling for Sensorimotor-Association axis. Among all receptors tested, $GABA_A$ ranked the highest (Fig. 3 D). Additionally, serotonergic receptors (5HT2A $r$ = -0.297, $P$ = 0.003, 5HT6 $r$ = -0.246, $P$ = 0.014, 5HT1b $r$ = -0.243, $P$ = 0.016, 5HTT $r$ = -0.218, $P$ = 0.030), dopamine transporter (DAT $r$ = -0.275, $P$ = 0.006), and metabotropic glutamate receptor 5 (mGluR5 $r$ = -0.255, $P$ = 0.011) showed significant correlations with alcohol effects.

Alcohol also significantly reduced the Hurst exponent in subcortical regions (Fig. S2C, $t$ = 10.36, $P$ < 0.001). Although no regions survived multiple comparison correction, the effect was most pronounced in the cerebellum, globus pallidus, nucleus accumbens, and substantia nigra (Fig. S2D).

## 4. Discussion

In this study, we tested the validity of the Hurst exponent as a marker of neural inhibition using alcohol as a pharmacological challenge across rats and humans. As predicted, alcohol exposure led to a reduction in the Hurst exponent, and these effects closely aligned with $GABA_A$ receptor expression across both species. Together, these findings provide evidence that the Hurst exponent reliably reflects reductions in inhibitory neuronal activity in a time-sensitive manner.

Our findings extend prior work on alcohol's effects, which has largely focused on prefrontal regions in rodents (Badanich et al., 2013; Li et al., 2021, 2002; Nimitvilai et al., 2017; Tu et al., 2007; Woodward and Pava, 2009), by demonstrating that alcohol's impact is widespread across the cortex. The spatial distribution of Hurst exponent reductions aligns with prior neuroimaging studies reporting widespread increases in cerebral blood flow (Marxen et al., 2014; Mathew and Wilson, 1986; Rickenbacher et al., 2011; Strang et al., 2015), and altered functional connectivity within visual, sensorimotor, and frontal networks in humans (Esposito et al., 2010; Khalili-Mahani et al., 2012; Ochi et al., 2022). Interestingly, alcohol's strongest effects appeared in sensory regions in rats but in association regions in humans, which may reflect species differences in the relative importance of these cortical systems. In humans, this spatial pattern echoes findings of alcohol-related cortical thinning and volume loss (Daviet et al., 2022), raising the possibility that acute neuronal hyperexcitability could contribute over time to structural vulnerability.

The spatial correlation between alcohol's effects on the Hurst exponent and $GABA_A$ receptor expression in both species further supports the specificity of the Hurst exponent in reflecting inhibitory neuronal activity, as alcohol's effects on inhibitory neurons are mediated by $GABA_A$ receptors (Diaz and Valenzuela, 2016; Jia et al., 2008; Liang et al., 2006). Beyond GABA, we also observed correlations between the Hurst exponent and serotonin 2A and dopamine transporter expression. These findings align with evidence that alcohol increases dopamine release in a dose-dependent manner (Aalto et al., 2015; Boileau et al., 2003; Urban et al., 2010; Yan, 1999; Yim et al., 1998; Yim and Gonzales, 2000; Yoshimoto et al., 1992) and that dopamine suppresses inhibition through D2 receptor signaling (Gorelova et al., 2002; Le Moine and Gaspar, 1998; Trantham-Davidson et al., 2004). Similarly, alcohol's

interactions with serotonin receptors (Lovinger, 1997; Lovinger and Peoples, 1993; Lovinger and Zhou, 1994) may contribute to its effects on inhibition. Notably, we did not observe a significant relationship between alcohol effects on the Hurst exponent and NMDA receptor expression, highlighting the specificity of the Hurst exponent for inhibitory neuronal activity, rather than excitatory neurons, whose responses to alcohol are primarily mediated through NMDA receptor antagonism (Badanich et al., 2013; Li et al., 2002).

We also detected reductions in the Hurst exponent in subcortical regions in rats, particularly in the cerebellum and striatum. These regions are critical to alcohol's motor and reward effects, consistent with mechanisms such as Purkinje cell disinhibition leading to ataxia (Mitoma et al., 2021) and striatal dopamine release driven by disinhibition of dopamine neurons (Charlet et al., 2011). Similar but nonsignificant trends were observed in humans. However, the validity of the Hurst exponent in subcortical regions remains uncertain, as differences in region size make averaged time series and resulting estimates difficult to compare across structures, and because the Hurst exponent in these regions has not been systematically validated in prior studies as a reliable marker of inhibitory neuronal activity.

Our study has several limitations. One challenge of the Hurst exponent is its susceptibility to motion artifacts. Compared to rats, alcohol's effects on the Hurst exponent in humans were relatively subtle, as no individual cortical or subcortical regions showed significant effects after correction for multiple comparisons. This may be due to the strong correlation between motion and the Hurst exponent, as alcohol increases motion and controlling for motion may have overly diminished the observed alcohol effect. Well-documented alcohol-induced changes in the cardiovascular system (Brunner et al., 2021; Lucas et al., 2005; Piano, 2017) could contribute to increased motion, underscoring the need for better understanding and control of these factors. In addition, our human fMRI protocol used multiband acceleration, which is associated with signal-to-noise ratio penalties particularly in subcortical structures (Seitzman et al., 2020; Srirangarajan et al., 2021), so our protocol could have limited our ability to detect effects of alcohol in subcortical regions.

Furthermore, the $GABA_A$ receptor expression data for both rats and humans were obtained from samples different from those used for fMRI and represent averages across individuals. Therefore, intra-individual variability in receptor expression was not possible to investigate. $GABA_A$ receptors have multiple subtypes, and acute alcohol primarily potentiates the α4βδ and α6βδ subtypes (Diaz and Valenzuela, 2016; Jia et al., 2008; Liang et al., 2006). In this study, flumazenil was used as a ligand for both rats and humans; however, it predominantly quantifies the α1–3βγ2 and α5βγ2 subtypes, which make up the majority of cortical $GABA_A$ receptors, rather than the α4βδ and α6βδ subtypes (Hanrahan et al., 2011; Wieland et al., 1992). Although examining a potential correlation between alcohol's effect on the Hurst exponent and the cortical expression of α4/6 subunits (Pirker et al., 2000) would be informative, such expression data are currently not available in a template space compatible with the fMRI data for either humans or rodents. Future work incorporating subtype-specific molecular maps may help clarify whether alcohol's effects on the Hurst exponent are preferentially related to these receptor subtypes.

Finally, we did not examine the behavioral consequences of the decrease in the Hurst exponent; therefore, the link between neural inhibition and behavioral inhibition remains unclear. Previous studies have reported that Hurst exponents are higher in low-impulsive compared with high-impulsive participants, suggesting that greater neural inhibition (reflected by a higher Hurst exponent) may be associated with greater behavioral inhibition (*i.e.*, lower impulsivity) (Akhrif et al., 2018). Other studies have shown that higher Hurst exponents are linked to faster response times for correct decisions in facial encoding task (Wink et al., 2008) and to greater performance improvements with training in for a variety of cognitive tasks (Kardan et al., 2023). Together, these findings suggest a possible link between higher Hurst exponents, which may indicate enhanced neural inhibitory capacity and an improved signal-to-noise ratio in neural activity, and better cognitive performance.

In summary, our findings provide cross-species evidence that the Hurst exponent reliably reflects reductions in inhibitory neuronal activity induced by alcohol. By integrating rodent and human data and linking alcohol's effects to $GABA_A$ receptor distributions, our results strengthen the evidence supporting the Hurst exponent as an *in vivo* fMRI marker of neural inhibition. These results not only advance the validation of the Hurst exponent but also illustrate how alcohol's widespread, multi-receptor effects offer a unique tool for probing inhibitory function in the human brain.

## Ethics statement

The animal data used in this study were originally collected as part of the study by Lee et al. (Lee et al., 2023). Studies involving animals were conducted in accordance with the Guide for the Care and Use of Laboratory Animals established by the National Institutes of Health, using protocols approved by the Institutional Animal Care and Use Committee of the University of North Carolina at Chapel Hill.

Studies involving human participants were conducted in accordance with the ethical standards of the institutional and/or national research committees and the 1964 Declaration of Helsinki and its later amendments or comparable ethical standards. Written informed consent was obtained from all participants, and the study was approved by the Institutional Review Board of the University of Pennsylvania.

## Data and code availability statement

All code used for the analyses is available on GitHub at https://github.com/monami-nishio/alcohol_effect_hurst and on Zenodo at https://doi.org/10.5281/zenodo.19020258.

## CRediT authorship contribution statement

**Monami Nishio:** Writing – original draft, Visualization, Methodology, Investigation, Formal analysis, Conceptualization. **Xinyi Wang:** Writing – review & editing, Methodology, Data curation. **Eli J. Cornblath:** Writing – review & editing, Methodology, Data curation. **Sung-Ho Lee:** Writing – review & editing, Data curation. **Yen-Yu Ian Shih:** Writing – review & editing, Data curation. **Nicola Palomero-Gallagher:** Writing – review & editing, Supervision, Methodology, Investigation, Data curation. **Michael J. Arcaro:** Writing – review & editing, Supervision. **David M. Lydon-Staley:** Writing – review & editing, Supervision, Methodology, Investigation, Funding acquisition, Data curation. **Allyson P. Mackey:** Writing – review & editing, Supervision, Project administration, Funding acquisition, Conceptualization.

## Declaration of competing interest

The authors declare no competing interests.

## Acknowledgements

We thank all of the individuals who participated in this research. This study was supported by a National Science Foundation CAREER award (to A.P.M. under Grant No 2045095), Brain & Behavior Research Foundation (to D.M.L.-S.), Quad Fellowship (to M.N.) and Nakajima Foundation Scholarship (to M.N.).

## Supplementary materials

Supplementary material associated with this article can be found, in the online version, at doi:10.1016/j.neuroimage.2026.121899.

## References


Aalto, S., Ingman, K., Alakurtti, K., Kaasinen, V., Virkkala, J., Någren, K., Rinne, J.O., Scheinin, H., 2015. Intravenous ethanol increases dopamine release in the ventral striatum in humans: PET study using bolus-plus-infusion administration of [11 C] raclopride. J. Perinatol. 35. https://doi.org/10.1038/jcbfm.2014.209.

Akhrif, A., Romanos, M., Domschke, K., Schmitt-Boehrer, A., Neufang, S., 2018. Fractal analysis of BOLD time series in a network associated with waiting impulsivity. Front. Physiol. 9. https://doi.org/10.3389/fphys.2018.01378.

Avants, B.B., Epstein, C.L., Grossman, M., Gee, J.C., 2008. Symmetric diffeomorphic image registration with cross-correlation: evaluating automated labeling of elderly and neurodegenerative brain. Med. Image Anal. 12. https://doi.org/10.1016/j.media.2007.06.004.

Avants, B.B., Yushkevich, P., Pluta, J., Minkoff, D., Korczykowski, M., Detre, J., Gee, J.C., 2010. The optimal template effect in hippocampus studies of diseased populations. Neuroimage 49. https://doi.org/10.1016/j.neuroimage.2009.09.062.

Badanich, K.A., Mulholland, P.J., Beckley, J.T., Trantham-Davidson, H., Woodward, J.J., 2013. Ethanol reduces neuronal excitability of lateral orbitofrontal cortex neurons via a glycine receptor dependent mechanism. Neuropsychopharmacology 38. https://doi.org/10.1038/npp.2013.12.

Boileau, I., Assaad, J.M., Pihl, R.O., Benkelfat, C., Leyton, M., Diksic, M., Tremblay, R.E., Dagher, A., 2003. Alcohol promotes dopamine release in the human nucleus accumbens. Synapse 49. https://doi.org/10.1002/syn.10226.

Broadwater, M.A., Lee, S.H., Yu, Y., Zhu, H., Crews, F.T., Robinson, D.L., Shih, Y.Y.I., 2018. Adolescent alcohol exposure decreases frontostriatal resting-state functional connectivity in adulthood. Addict. Biol. 23. https://doi.org/10.1111/adb.12530.

Brunner, S., Winter, R., Werzer, C., von Stülpnagel, L., Clasen, I., Hameder, A., Stöver, A., Graw, M., Bauer, A., Sinner, M.F., 2021. Impact of acute ethanol intake on cardiac autonomic regulation. Sci. Rep. 11. https://doi.org/10.1038/s41598-021-92767-y.

Charlet, K., Beck, A., Heinz, A., 2011. The dopamine system in mediating alcohol effects in humans. Curr. Top. Behav. Neurosci. 13. https://doi.org/10.1007/7854_2011_130.

Chen, Z., Hu, K., Carpena, P., Bernaola-Galvan, P., Stanley, H.E., Ivanov, P.C., 2005. Effect of nonlinear filters on detrended fluctuation analysis. Phys. Rev. e Stat. Nonlin. Soft. Matter. Phys. 71. https://doi.org/10.1103/PhysRevE.71.011104.

Chini, M., Pfeffer, T., Hanganu-Opatz, I., 2022. An increase of inhibition drives the developmental decorrelation of neural activity. Elife 11. https://doi.org/10.7554/eLife.78811.

Churchill, N.W., Spring, R., Grady, C., Cimprich, B., Askren, M.K., Reuter-Lorenz, P.A., Jung, M.S., Peltier, S., Strother, S.C., Berman, M.G., 2016. The suppression of scale-free fMRI brain dynamics across three different sources of effort: aging, task novelty and task difficulty. Sci. Rep. 6. https://doi.org/10.1038/srep30895.

Ciric, R., Rosen, A.F.G., Erus, G., Cieslak, M., Adebimpe, A., Cook, P.A., Bassett, D.S., Davatzikos, C., Wolf, D.H., Satterthwaite, T.D., 2018. Mitigating head motion artifact in functional connectivity MRI. Nat. Protoc. 13. https://doi.org/10.1038/s41596-018-0065-y.

Cox, R.W., 1996. AFNI: software for analysis and visualization of functional magnetic resonance neuroimages. Comput. Biomed. Res. 29. https://doi.org/10.1006/cbmr.1996.0014.

Cox, R.W., Hyde, J.S., 1997. Software tools for analysis and visualization of fMRI data. NMR Biomed. 10. https://doi.org/10.1002/(SICI)1099-1492.(199706/08)10:4/5<171::AID-BM453>3.0.CO;2-L.

Dale, A.M., Fischl, B., Sereno, M.I., 1999. Cortical surface-based analysis: I. Segmentation and surface reconstruction. Neuroimage 9. https://doi.org/10.1006/nimg.1998.0395.

Daviet, R., Aydogan, G., Jagannathan, K., Spilka, N., Koellinger, P.D., Kranzler, H.R., Nave, G., Wetherill, R.R., 2022. Associations between alcohol consumption and gray and white matter volumes in the UK Biobank. Nat. Commun. 13. https://doi.org/10.1038/s41467-022-28735-5.

Diaz, M.R., Valenzuela, C.F., 2016. Sensitivity of GABAergic tonic currents to acute ethanol in cerebellar granule neurons is not age- or δ subunit-dependent in developing rats. Alcohol Clin. Exp. Res. 40. https://doi.org/10.1111/acer.12940.

Esposito, F., Pignataro, G., Di Renzo, G., Spinali, A., Paccone, A., Tedeschi, G., Annunziato, L., 2010. Alcohol increases spontaneous BOLD signal fluctuations in the visual network. Neuroimage 53. https://doi.org/10.1016/j.neuroimage.2010.06.061.

Esteban, O., Markiewicz, C.J., Blair, R.W., Moodie, C.A., Isik, A.I., Erramuzpe, A., Kent, J. D., Goncalves, M., DuPre, E., Snyder, M., Oya, H., Ghosh, S.S., Wright, J., Durnez, J., Poldrack, R.A., Gorgolewski, K.J., 2019. fMRIPrep: a robust preprocessing pipeline for functional MRI. Nat. Methods 16. https://doi.org/10.1038/s41592-018-0235-4.

Fernando Valenzuela, C., 1997. Alcohol and neurotransmitter interactions. Alcohol Res. Health 21.

Flandrin, P., 1992. Wavelet analysis and synthesis of fractional brownian motion. IEEe Trans. Inf. Theory. 38. https://doi.org/10.1109/18.119751.

Fonov, V., Evans, A.C., Botteron, K., Almli, C.R., McKinstry, R.C., Collins, D.L., 2011. Unbiased average age-appropriate atlases for pediatric studies. Neuroimage 54. https://doi.org/10.1016/j.neuroimage.2010.07.033.

Gao, R., Peterson, E.J., Voytek, B., 2017. Inferring synaptic excitation/inhibition balance from field potentials. Neuroimage 158. https://doi.org/10.1016/j.neuroimage.2017.06.078.

Gerner, R.H., Hare, T.A., 1981. CSF GABA in normal subjects and patients with depression, schizophrenia, mania, and anorexia nervosa. Am. J. Psychiatry 138. https://doi.org/10.1176/ajp.138.8.1098.

Gorelova, N., Seamans, J.K., Yang, C.R., 2002. Mechanisms of dopamine activation of fast-spiking interneurons that exert inhibition in rat prefrontal cortex. J. Neurophysiol. 88. https://doi.org/10.1152/jn.00335.2002.

Gorgolewski, K.J., Auer, T., Calhoun, V.D., Craddock, R.C., Das, S., Duff, E.P., Flandin, G., Ghosh, S.S., Glatard, T., Halchenko, Y.O., Handwerker, D.A., Hanke, M., Keator, D., Li, X., Michael, Z., Maumet, C., Nichols, B.N., Nichols, T.E., Pellman, J., Poline, J.B., Rokem, A., Schaefer, G., Sochat, V., Triplett, W., Turner, J.A., Varoquaux, G., Poldrack, R.A., 2016. The brain imaging data structure, a format for organizing and describing outputs of neuroimaging experiments. Sci. Data 3. https://doi.org/10.1038/sdata.2016.44.

Greve, D.N., Fischl, B., 2009. Accurate and robust brain image alignment using boundary-based registration. Neuroimage 48. https://doi.org/10.1016/j.neuroimage.2009.06.060.

Haghir, H., Kuckertz, A., Zhao, L., Hami, J., Palomero-Gallagher, N., 2023. A new map of the rat isocortex and proisocortex: cytoarchitecture and M2 receptor distribution patterns. Brain Struct. Funct. https://doi.org/10.1007/s00429-023-02654-7.

Han, J., Keedy, S., Murray, C.H., Foxley, S., de Wit, H., 2021. Acute effects of alcohol on resting-state functional connectivity in healthy young men. Addict. Behav. 115. https://doi.org/10.1016/j.addbeh.2020.106786.

Hanrahan, J.R., Chebib, M., Johnston, G.A.R., 2011. Flavonoid modulation of GABA A receptors. Br. J. Pharmacol. https://doi.org/10.1111/j.1476-5381.2011.01228.x.

Hansen, J.Y., Shafiei, G., Markello, R.D., Smart, K., Cox, S.M.L., Nørgaard, M., Beliveau, V., Wu, Y., Gallezot, J.D., Aumont, É., Servaes, S., Scala, S.G., DuBois, J.M., Wainstein, G., Bezgin, G., Funck, T., Schmitz, T.W., Spreng, R.N., Galovic, M., Koepp, M.J., Duncan, J.S., Coles, J.P., Fryer, T.D., Aigbirhio, F.I., McGinnity, C.J., Hammers, A., Soucy, J.P., Baillet, S., Guimond, S., Hietala, J., Bedard, M.A., Leyton, M., Kobayashi, E., Rosa-Neto, P., Ganz, M., Knudsen, G.M., Palomero-Gallagher, N., Shine, J.M., Carson, R.E., Tuominen, L., Dagher, A., Misic, B., 2022. Mapping neurotransmitter systems to the structural and functional organization of the human neocortex. Nat. Neurosci. 25. https://doi.org/10.1038/s41593-022-01186-3.

Hanson, J.L., Nacewicz, B.M., 2021. Amygdala allostasis and early life adversity: considering excitotoxicity and inescapability in the sequelae of stress. Front. Hum. Neurosci. 15. https://doi.org/10.3389/fnhum.2021.624705.

He, B.J., 2011. Scale-free properties of the functional magnetic resonance imaging signal during rest and task. J. Neurosci. 31. https://doi.org/10.1523/JNEUROSCI.2111-11.2011.

Hensch, T.K., 2005. Critical period plasticity in local cortical circuits. Nat. Rev. Neurosci. 6. https://doi.org/10.1038/nrn1787.

Hsu, L.M., Wang, S., Ranadive, P., Ban, W., Chao, T.H.H., Song, S., Cerri, D.H., Walton, L. R., Broadwater, M.A., Lee, S.H., Shen, D., Shih, Y.Y.I., 2020. Automatic skull stripping of rat and mouse brain MRI data using U-net. Front. Neurosci. 14. https://doi.org/10.3389/fnins.2020.568614.

Hu, K., Ivanov, P.C., Chen, Z., Carpena, P., Stanley, H.E., 2001. Effect of trends on detrended fluctuation analysis. Phys. Rev. e Stat. Phys. Plasmas. Fluids. Relat. Interdiscip. Topics. 64. https://doi.org/10.1103/PhysRevE.64.011114.

Impieri, D., Zilles, K., Niu, M., Rapan, L., Schubert, N., Galletti, C., Palomero-Gallagher, N., 2019. Receptor density pattern confirms and enhances the anatomic-functional features of the macaque superior parietal lobule areas. Brain Struct. Funct 224. https://doi.org/10.1007/s00429-019-01930-9.

Ivanov, P.C., Nunes Amaral, L.A., Goldberger, A.L., Havlin, S., Rosenblum, M.G., Stanley, H.E., Struzik, Z.R., 2001. From 1/f noise to multifractal cascades in heartbeat dynamics. Chaos. 11. https://doi.org/10.1063/1.1395631.

Jenkinson, M., Bannister, P., Brady, M., Smith, S., 2002. Improved optimization for the robust and accurate linear registration and motion correction of brain images. Neuroimage 17. https://doi.org/10.1016/S1053-8119-(02)91132-8.

Jia, F., Chandra, D., Homanics, G.E., Harrison, N.L., 2008. Ethanol modulates synaptic and extrasynaptic GABAA receptors in the thalamus. J. Pharmacol. Exp. Ther. 326. https://doi.org/10.1124/jpet.108.139303.

Kardan, O., Stier, A.J., Layden, E.A., Choe, K.W., Lyu, M., Zhang, X., Beilock, S.L., Rosenberg, M.D., Berman, M.G., 2023. Improvements in task performance after practice are associated with scale-free dynamics of brain activity. Net. Neurosci. 7. https://doi.org/10.1162/netn_a_00319.

Khalili-Mahani, N., Zoethout, R.M.W., Beckmann, C.F., Baerends, E., de Kam, M.L., Soeter, R.P., Dahan, A., van Buchem, M.A., van Gerven, J.M.A., Rombouts, S.A.R.B., 2012. Effects of morphine and alcohol on functional brain connectivity during "resting state": a placebo-controlled crossover study in healthy young men. Hum. Brain Mapp. 33. https://doi.org/10.1002/hbm.21265.

Klein, A., Ghosh, S.S., Bao, F.S., Giard, J., Häme, Y., Stavsky, E., Lee, N., Rossa, B., Reuter, M., Chaibub Neto, E., Keshavan, A., 2017. Mindboggling morphometry of human brains. PLoS. Comput. Biol. 13. https://doi.org/10.1371/journal.pcbi.1005350.

Kotoula, V., Evans, J.W., Punturieri, C.E., Zarate, C.A., 2023. Review: the use of functional magnetic resonance imaging (fMRI) in clinical trials and experimental research studies for depression. Front. NeuroimAging. https://doi.org/10.3389/fnimg.2023.1110258.

Larsen, B., Cui, Z., Adebimpe, A., Pines, A., Alexander-Bloch, A., Bertolero, M., Calkins, M.E., Gur, R.E., Gur, R.C., Mahadevan, A.S., Moore, T.M., Roalf, D.R., Seidlitz, J., Sydnor, V.J., Wolf, D.H., Satterthwaite, T.D., 2022. A developmental reduction of the excitation:inhibition ratio in association cortex during adolescence. Sci. Adv. 8. https://doi.org/10.1126/sciadv.abj8750.

Le Moine, C., Gaspar, P., 1998. Subpopulations of cortical GABAergic interneurons differ by their expression of D1 and D2 dopamine receptor subtypes. Mol. Brain Res. 58. https://doi.org/10.1016/S0169-328X.(98)00118-1.

Lee, S.H., Broadwater, M.A., Ban, W., Wang, T.W.W., Kim, H.J., Dumas, J.S., Vetreno, R. P., Herman, M.A., Morrow, A.L., Besheer, J., Kash, T.L., Boettiger, C.A., Robinson, D. L., Crews, F.T., Shih, Y.Y.I., 2021. An isotropic EPI database and analytical pipelines for rat brain resting-state fMRI. Neuroimage 243. https://doi.org/10.1016/j.neuroimage.2021.118541.

Lee, S.H., Shnitko, T.A., Hsu, L.M., Broadwater, M.A., Sardinas, M., Wang, T.W.W., Robinson, D.L., Vetreno, R.P., Crews, F.T., Shih, Y.Y.I., 2023. Acute alcohol induces greater dose-dependent increase in the lateral cortical network functional connectivity in adult than adolescent rats. Addict. Neurosci. 7. https://doi.org/10.1016/j.addicn.2023.100105.

Li, M., Cabrera-Garcia, D., Salling, M.C., Au, E., Yang, G., Harrison, N.L., 2021. Alcohol reduces the activity of somatostatin interneurons in the mouse prefrontal cortex: a neural basis for its disinhibitory effect? Neuropharmacology. 188. https://doi.org/10.1016/j.neuropharm.2021.108501.

Li, Q., Wilson, W.A., Scott Swartzwelder, H., 2002. Differential effect of ethanol on NMDA EPSCs in pyramidal cells in the posterior cingulate cortex of juvenile and adult rats. J. Neurophysiol. 87. https://doi.org/10.1152/jn.00433.2001.

Liang, J., Zhang, N., Cagetti, E., Houser, C.R., Olsen, R.W., Spigelman, I., 2006. Chronic intermittent ethanol-induced switch of ethanol actions from extrasynaptic to synaptic hippocampal GABAA receptors. J. Neurosci. 26. https://doi.org/10.1523/JNEUROSCI.4702-05.2006.

Linke, A.C., Chen, B., Olson, L., Cordova, M., Wilkinson, M., Wang, T., Herrera, M., Salmina, M., Rios, A., Mahmalji, J., Do, T., Vu, J., Budman, M., Walker, A., Fishman, I., 2024. Altered development of the Hurst Exponent in medial prefrontal cortex in preschoolers with autism. Biol. Psychiatry Cogn. Neurosci. Neuroimaging 10. https://doi.org/10.1016/j.bpsc.2024.09.003.

Linkenkaer-Hansen, K., Nikouline, V.V., Palva, J.M., Ilmoniemi, R.J., 2001. Long-range temporal correlations and scaling behavior in human brain oscillations. J. Neurosci. 21. https://doi.org/10.1523/jneurosci.21-04-01370.2001.

Liu, Y., Ouyang, P., Zheng, Y., Mi, L., Zhao, J., Ning, Y., Guo, W., 2021. A selective review of the excitatory-inhibitory imbalance in schizophrenia: underlying biology, genetics, microcircuits, and symptoms. Front. Cell Dev. Biol. 9. https://doi.org/10.3389/fcell.2021.664535.

Lombardi, F., Herrmann, H.J., de Arcangelis, L., 2017. Balance of excitation and inhibition determines 1/f power spectrum in neuronal networks. Chaos. 27. https://doi.org/10.1063/1.4979043.

Lovinger, D.M., 1997. Serotonin's role in alcohol's effects on the brain. Alcohol Res. Health 21.

Lovinger, D.M., Peoples, R.W., 1993. Actions of alcohols and other sedative/hypnotic compounds on cation channels associated with glutamate and 5-HT3 receptors. Alcohol, Cell Membranes, and Signal Transduction in Brain. Springer, Boston, MA. https://doi.org/10.1007/978-1-4615-2470-0_14.

Lovinger, D.M., Zhou, Q., 1994. Alcohols potentiate ion current mediated by recombinant 5-HT3RA receptors expressed in a mammalian cell line. Neuropharmacology 33. https://doi.org/10.1016/0028-3908.(94)90131-7.

Lu, H., Zou, Q., Gu, H., Raichle, M.E., Stein, E.A., Yang, Y., 2012. Rat brains also have a default mode network. Proc. Natl. Acad. Sci. u S. a 109. https://doi.org/10.1073/pnas.1200506109.

Lucas, D.L., Brown, R.A., Wassef, M., Giles, T.D., 2005. Alcohol and the cardiovascular system: research challenges and opportunities. J. Am. Coll. Cardiol. 45. https://doi.org/10.1016/j.jacc.2005.02.075.

Marxen, M., Gan, G., Schwarz, D., Mennigen, E., Pilhatsch, M., Zimmermann, U.S., Guenther, M., Smolka, M.N., 2014. Acute effects of alcohol on brain perfusion monitored with arterial spin labeling magnetic resonance imaging in young adults. J. Cereb. Blood Flow Metab. 34. https://doi.org/10.1038/jcbfm.2013.223.

Mathew, R.J., Wilson, W.H., 1986. Regional cerebral blood flow changes associated with ethanol intoxication. Stroke 17. https://doi.org/10.1161/01.STR.17.6.1156.

McCarthy, D.M., Zhang, X., Darnell, S.B., Sangrey, G.R., Yanagawa, Y., Sadri-Vakili, G., Bhide, P.G., 2011. Cocaine alters BDNF expression and neuronal migration in the embryonic mouse forebrain. J. Neurosci. 31. https://doi.org/10.1523/JNEUROSCI.2944-11.2011.

Mitoma, H., Manto, M., Shaikh, A.G., 2021. Mechanisms of ethanol-induced cerebellar ataxia: underpinnings of neuronal death in the cerebellum. Int. J. Environ. Res. Public Health. https://doi.org/10.3390/ijerph18168678.

National Highway Traffic Safety Administration, 2022. Drunk driving.

National Institute on Alcohol Abuse and Alcoholism, 2022. Alcohol's Effects on Health: Research-based Information on Drinking and It's Impact. National Institute on Alcohol Abuse and Alcoholism, Bathesda, MD.

Nimitvilai, S., Uys, J.D., Woodward, J.J., Randall, P.K., Ball, L.E., Williams, R.W., Jones, B.C., Lu, L., Grant, K.A., Mulholland, P.J., 2017. Orbitofrontal neuroadaptations and cross-species synaptic biomarkers in heavy-drinking macaques. J. Neurosci. 37. https://doi.org/10.1523/JNEUROSCI.0133-17.2017.

Nishio, M., Ellwood-Lowe, M., Woodburn, M., McDermott, C., Park, A., Tooley, U., Boroshok, A., Grandjean, J., Mackey, A., 2025. The development of neural inhibition across species: insights from the Hurst exponent. J. Neurosci. 45. https://doi.org/10.1523/JNEUROSCI.0025-25.2025.

Ochi, R., Ueno, F., Sakuma, M., Tani, H., Tsugawa, S., Graff-Guerrero, A., Uchida, H., Mimura, M., Oshima, S., Matsushita, S., Nakajima, S., 2022. Patterns of functional connectivity alterations induced by alcohol reflect somatostatin interneuron expression in the human cerebral cortex. Sci. Rep. 12. https://doi.org/10.1038/s41598-022-12035-5.

Palomero-Gallagher, N., Schleicher, A., Lindemann, S., Lessenich, A., Zilles, K., Löscher, W., 2008. Receptor fingerprinting the circling ci2 rat mutant: insights into brain asymmetry and motor control. Exp. Neurol. 210. https://doi.org/10.1016/j.expneurol.2007.12.014.

Palomero-Gallagher, N., Schleicher, A.A., Zilles, K., Löscher, W., 2010. The circling ci2 rat mutant revisited: receptor architecture of the motor cortex. Neuroscience 170. https://doi.org/10.1016/j.neuroscience.2010.07.043.

Paxinos, G., Watson, C., 2014. The Rat Brain in Stereotaxic Coordinates Seventh Edition. Elsevier Academic Press, San Diego, CA, p. 170.

Peng, C.K., Buldyrev, S.V., Havlin, S., Simons, M., Stanley, H.E., Goldberger, A.L., 1994. Mosaic organization of DNA nucleotides. Phys. Rev. e 49. https://doi.org/10.1103/PhysRevE.49.1685.

Piano, M.R., 2017. Alcohol's effects on the cardiovascular system. Alcohol Res. 38. https://doi.org/10.35946/arcr.v38.2.06.

Pirker, S., Schwarzer, C., Wieselthaler, A., Sieghart, W., Sperk, G., 2000. GABA (A) receptors: immunocytochemical distribution of 13 subunits in the adult rat brain. Neuroscience 101. https://doi.org/10.1016/S0306-4522.(00)00442-5.

Power, J.D., Mitra, A., Laumann, T.O., Snyder, A.Z., Schlaggar, B.L., Petersen, S.E., 2014. Methods to detect, characterize, and remove motion artifact in resting state fMRI. Neuroimage 84. https://doi.org/10.1016/j.neuroimage.2013.08.048.

Rehman, N., Mandic, D.P., 2010. Multivariate empirical mode decomposition. *Proceedings of the royal society* 466. https://doi.org/10.1016/j.ymssp.2016.03.010.

Rickenbacher, E., Greve, D.N., Azma, S., Pfeuffer, J., Marinkovic, K., 2011. Effects of alcohol intoxication and gender on cerebral perfusion: an arterial spin labeling study. Alcohol 45. https://doi.org/10.1016/j.alcohol.2011.04.002.

Saunders, J.B., Aasland, O.G., Babor, T.F., De La Fuente, J.R., Grant, M., 1993. Development of the Alcohol Use Disorders Identification Test (AUDIT): WHO Collaborative Project on Early detection of persons with harmful alcohol consumption-II. Addiction 88. https://doi.org/10.1111/j.1360-0443.1993.tb02093.x.

Schaefer, A., Kong, R., Gordon, E.M., Laumann, T.O., Zuo, X.-N., Holmes, A.J., Eickhoff, S.B., Yeo, B.T.T., 2018. Local-global parcellation of the Human cerebral cortex from intrinsic functional connectivity MRI. Cerebral Cortex 28. https://doi.org/10.1093/cercor/bhx179.

Schmitt, D.T., Ivanov, P.C., 2007. Fractal scale-invariant and nonlinear properties of cardiac dynamics remain stable with advanced age: a new mechanistic picture of cardiac control in healthy elderly. Am. J. Physiol. Regul. Integr. Comp. Physiol. 293. https://doi.org/10.1152/ajpregu.00372.2007.

Schmitt, D.T., Stein, P.K., Ivanov, P.C., 2009. Stratification pattern of static and scale-invariant dynamic measures of heartbeat fluctuations across sleep stages in young and elderly. IEEE Trans. Biomed. Eng. 56. https://doi.org/10.1109/TBME.2009.2014819.

Shenoda, B.B., 2017. An overview of the mechanisms of abnormal GABAergic interneuronal cortical migration associated with prenatal ethanol exposure. Neurochem. Res. 42. https://doi.org/10.1007/s11064-016-2169-5.

Seitzman, B.A., Gratton, C., Marek, S., Raut, R.V., Dosenbach, N.U.F., Schlaggar, B.L., Petersen, S.E., Greene, DJ., 2020. A set of functionally-defined brain regions with improved representation of the subcortex and cerebellum. Neuroimage 206. https://doi.org/10.1016/j.neuroimage.2019.116290.

Shnitko, T.A., Kennerly, L.C., Spear, L.P., Robinson, D.L., 2014. Ethanol reduces evoked dopamine release and slows clearance in the rat medial prefrontal cortex. Alcohol Clin. Exp. Res. 38. https://doi.org/10.1111/acer.12587.

Shnitko, T.A., Spear, L.P., Robinson, D.L., 2016. Adolescent binge-like alcohol alters sensitivity to acute alcohol effects on dopamine release in the nucleus accumbens of adult rats. Psychopharmacology. (Berl) 233. https://doi.org/10.1007/s00213-015-4106-8.

Sontate, K.V., Rahim Kamaluddin, M., Naina Mohamed, I., Mohamed, R.M.P., Shaikh, M. F., Kamal, H., Kumar, J., 2021. Alcohol, aggression, and violence: from public health to neuroscience. Front. Psychol. 12. https://doi.org/10.3389/fpsyg.2021.699726.

Srirangarajan, T., Mortazavi, L., Bortolini, T., Moll, J., Knutson, B., 2021. Multi-band FMRI compromises detection of mesolimbic reward responses. Neuroimage 244. https://doi.org/10.1016/j.neuroimage.2021.118617.

Strang, N.M., Claus, E.D., Ramchandani, V.A., Graff-Guerrero, A., Boileau, I., Hendershot, C.S., 2015. Dose-dependent effects of intravenous alcohol administration on cerebral blood flow in young adults. Psychopharmacology. (Berl) 232. https://doi.org/10.1007/s00213-014-3706-z.

Sydnor, V.J., Larsen, B., Bassett, D.S., Alexander-Bloch, A., Fair, D.A., Liston, C., Mackey, A.P., Milham, M.P., Pines, A., Roalf, D.R., Seidlitz, J., Xu, T., Raznahan, A., Satterthwaite, T.D., 2021. Neurodevelopment of the association cortices: patterns, mechanisms, and implications for psychopathology. Neuron 109. https://doi.org/10.1016/j.neuron.2021.06.016.

Tognarelli, J.M., Dawood, M., Shariff, M.I.F., Grover, V.P.B., Crossey, M.M.E., Cox, I.J., Taylor-Robinson, S.D., McPhail, M.J.W., 2015. Magnetic resonance spectroscopy: principles and techniques: lessons for clinicians. J. Clin. Exp. Hepatol. 5. https://doi.org/10.1016/j.jceh.2015.10.006.

Trakoshis, S., Martínez-Cañada, P., Rocchi, F., Canella, C., You, W., Chakrabarti, B., Ruigrok, A.N.V., Bullmore, E.T., Suckling, J., Markicevic, M., Zerbi, V., Baron-Cohen, S., Gozzi, A., Lai, M.C., Panzeri, S., Lombardo, M.V., 2020. Intrinsic excitation-inhibition imbalance affects medial prefrontal cortex differently in autistic men *versus* women. Elife 9. https://doi.org/10.7554/ELIFE.55684.

Trantham-Davidson, H., Neely, L.C., Lavin, A., Seamans, J.K., 2004. Mechanisms underlying differential D1 *versus* D2 dopamine receptor regulation of inhibition in prefrontal cortex. J. Neurosci. 24. https://doi.org/10.1523/JNEUROSCI.3179-04.2004.

Tu, Y., Kroener, S., Abernathy, K., Lapish, C., Seamans, J., Chandler, L.J., Woodward, J. J., 2007. Ethanol inhibits persistent activity in prefrontal cortical neurons. J. Neurosci. 27. https://doi.org/10.1523/JNEUROSCI.5378-06.2007.

Tustison, N.J., Avants, B.B., Cook, P.A., Zheng, Y., Egan, A., Yushkevich, P.A., Gee, J.C., 2010. N4ITK: improved N3 bias correction. IEEe Trans. Med. ImAging 29. https://doi.org/10.1109/TMI.2010.2046908.

Urban, N.B.L., Kegeles, L.S., Slifstein, M., Xu, X., Martinez, D., Sakr, E., Castillo, F., Moadel, T., O'Malley, S.S., Krystal, J.H., Abi-Dargham, A., 2010. Sex differences in striatal dopamine release in young adults after oral alcohol challenge: a positron emission tomography imaging study with [11C]raclopride. Biol. Psychiatry 68. https://doi.org/10.1016/j.biopsych.2010.06.005.

Vanderwal, T., Kelly, C., Eilbott, J., Mayes, L.C., Castellanos, F.X., 2015. Inscapes: a movie paradigm to improve compliance in functional magnetic resonance imaging. Neuroimage 122. https://doi.org/10.1016/j.neuroimage.2015.07.069.

Wieland, H.A., Lüddens, H., Seeburg, P.H., 1992. A single histidine in GABAA receptors is essential for benzodiazepine agonist binding. J. Biol. Chem. 267. https://doi.org/10.1016/s0021-9258.(18)45961-3.

Wink, A.M., Bullmore, E., Barnes, A., Bernard, F., Suckling, J., 2008. Monofractal and multifractal dynamics of low frequency endogenous brain oscillations in functional MRI. Hum. Brain Mapp. 29. https://doi.org/10.1002/hbm.20593.

Woodward, J.J., Pava, M.J., 2009. Effects of ethanol on persistent activity and up-states in excitatory and inhibitory neurons in prefrontal cortex. Alcohol Clin. Exp. Res. 33. https://doi.org/10.1111/j.1530-0277.2009.01059.x.

Yan, Q.S., 1999. Extracellular dopamine and serotonin after ethanol monitored with 5-minute microdialysis. Alcohol 19. https://doi.org/10.1016/S0741-8329.(99)00006-3.

Yim, H.J., Gonzales, R.A., 2000. Ethanol-induced increases in dopamine extracellular concentration in rat nucleus accumbens are accounted for by increased release and not uptake inhibition. Alcohol 22. https://doi.org/10.1016/S0741-8329.(00)00121-X.

Yim, H.J., Schallert, T., Randall, P.K., Gonzales, R.A., 1998. Comparison of local and systemic ethanol effects on extracellular dopamine concentration in rat nucleus accumbens by microdialysis. Alcohol. Clin. Exp. Res. https://doi.org/10.1111/j.1530-0277.1998.tb03662.x.

Yoshimoto, K., McBride, W.J., Lumeng, L., Li, T.K., 1992. Alcohol stimulates the release of dopamine and serotonin in the nucleus accumbens. Alcohol 9. https://doi.org/10.1016/0741-8329.(92)90004-T.

You, W., Achard, S., Stadler, J., Brückner, B., Seiffert, U., 2012. Fractal analysis of resting state functional connectivity of the brain. In: Proceedings of the International Joint Conference on Neural Networks. https://doi.org/10.1109/IJCNN.2012.6252657.

Yushkevich, P.A., Piven, J., Hazlett, H.C., Smith, R.G., Ho, S., Gee, J.C., Gerig, G., 2006. User-guided 3D active contour segmentation of anatomical structures: significantly improved efficiency and reliability. Neuroimage 31. https://doi.org/10.1016/j.neuroimage.2006.01.015.

Zhang, Y., Brady, M., Smith, S., 2001. Segmentation of brain MR images through a hidden Markov random field model and the expectation-maximization algorithm. IEEe Trans. Med. ImAging 20. https://doi.org/10.1109/42.906424.